12FTM15

American
Gear Manufacturers
Association

Technical Resources

AGMA Technical Paper

New Methods for the Calculation of the Load Capacity of Bevel and Hypoid Gears

By C. Wirth and B.-R. Höhn, ZG- Zahnräder und Getriebe GmbH, and C. Braykoff, MAN Truck & Bus AG

New Methods for the Calculation of the Load Capacity of Bevel and Hypoid Gears

Dr.-Ing. Christian Wirth and Prof. Dr.-Ing. Bernd-Robert Höhn, ZG- Zahnräder und Getriebe GmbH, and Dr.-Ing. Ch. Braykoff, MAN Truck & Bus AG

Abstract

A failure mode called “flank breakage” is increasingly observed in different applications of cylindrical and bevel gears. These breakages typically start from the active flank approximately in the middle of the active tooth height and propagate to the tooth root of the unloaded flank side. Crack initiation can be localized below the surface in the region between case and core of surface hardened gears. This failure mode can neither be explained by the known mechanism of tooth root breakage nor by the mechanism of pitting. Even bevel gears in truck and bus applications are at the risk to suffer from subsurface fatigue, if the optimum utilization of the material should be achieved. In this case a balance between the flank breakage and pitting risk has to be found. The purpose of this paper is to describe a new material, physically based calculation method to evaluate the risk of flank breakage versus the risk of pitting. The verification of this new method by experimental tests is exemplarily shown.

American Gear Manufacturers Association
1001 N. Fairfax Street, Suite 500
Alexandria, Virginia 22314

October 2012

ISBN: 978-1-61481-046-9

New Methods for the Calculation of the Load Capacity of Bevel and Hypoid Gears

Dr.-Ing. Christian Wirth and Prof. Dr.-Ing. Bernd-Robert Höhn, ZG- Zahnräder und Getriebe GmbH, and Dr.-Ing. Ch. Braykoff, MAN Truck & Bus AG

Introduction

A failure mode called "flank breakage" is increasingly observed in different applications of cylindrical and bevel gears. These breakages typically start from the active flank approximately in the middle of the active tooth height and propagate to the tooth root of the unloaded flank side.

Crack initiation can be localized below the surface in the region between case and core of surface hardened gears. This failure mode can neither be explained by the known mechanism of tooth root breakage nor by the mechanism of pitting. Even bevel gears in truck and bus applications are at the risk to suffer from subsurface fatigue, if the optimum utilization of the material should be achieved. In this case a balance between the flank breakage and pitting risk has to be found. The purpose of this paper is to describe a new material-physically based calculation method to evaluate the risk of flank breakage versus the risk of pitting. The method was used to improve the design of a gear set that failed in several cases by flank breakage on the wheel in test vehicles of MAN Truck & Bus (MTB). In Figure 1 a typically damaged tooth on the wheel is shown. In some cases pitting occurred on the coast flanks of the wheel (see Figure 1 right). It was possible to increase the load capacity of the wheel regarding pitting and flank breakage by means of the new method. Previous test runs approved this method.

Flank breakage in bevel gears

Flank breakage often appears without any other surface failures such as scuffing, pitting or micropitting. In some cases only one tooth is affected but usually more than one tooth fail as shown in Figure 2. Non-adequate material properties and heat treatment were expected to increase the risk of flank breakage, especially too low core strength and toughness, or too low or too high case depths [4] [5]. In many American publications flank breakage is also called "subsurface fatigue" or "subcase fatigue". In these papers the flank pressure is also regarded as the decisive parameter [2] [6] [13] [15] [16].

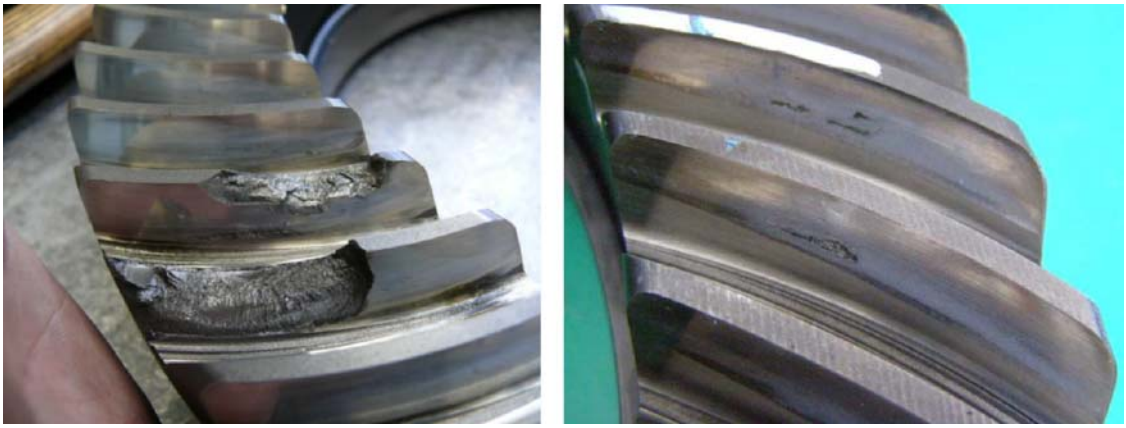

Figure 1. Flank breakage and pitting on the wheel

Figure 2. Flank breakage on two different wheels

Annast [1] investigated on basis of systematic tests the influence parameters on flank breakage on bevel gears. Annast identifies besides the known influence of the load conditions especially the case depth and the core hardness as an important parameter. Analysis of damage patterns of test and practical gears showed that the initiating crack always started below the surface in the region of the transition from case to core. For unidirectional loading the crack propagates to the active flank on the one side and to the tooth root on the other side. Annast analyzed the subsurface stresses with ROSLCOR [9] [17] by using the shear stress intensity hypothesis according to Tobie [18]. Oster [17] defined on basis of [21] a feasibility to consider compressive stresses in the case for the evaluation of the material exposure. Tobie expanded this method with the possibility to regard also tensile residual stresses (in the core). However the magisterial influence of tensile residual stresses pretended by the model according to Tobie, could not be approved by any other investigation (e.g., ANSI/AGMA 2003-B97). Therefore, Annast argued that it is sufficient to analyze only the section between the flank surface and the transient region of case and core. Tensile residual stresses were therefore not examined by Annast. In his proposed standard capable method only the region of the transition is regarded. A critical ratio between the acting maximum shear stress and the core hardness was derived out of the test gears and practical applications. If the ratio exceeds the limit the risk of flank breakage is considered as high.

Because of the uncertainties in the methods described above a new calculation method was proposed by Wirth [20] for the rating of bevel and hypoid gears. The method is based on Oster's and Hertter's [8] work. Hertter proposed for cylindrical gears an enhanced shear stress intensity hypothesis to evaluate the subsurface stresses even under consideration of compressive and tensile residual stresses. A separated examination of dynamic and static exposure allows to regard fatigue failures as well as failures from yielding. Because the local allowable strength values in the considered material element are derived from the hardness by means of material-physical relations the new method is named "material-physically based calculation method". Wirth transferred Hertter's method to bevel and hypoid gears considering their specifics as for example the sliding conditions.

Material-physically based calculation method for bevel and hypoid gears

The material-physically based calculation method allows the consideration of complex stress conditions beneath the flank surface that are caused by the load and the heat treatment process. The permissible stresses are derived from the hardness values and material-physical parameters. The occurring stresses are compared with the permissible stresses in discrete sections in the material. On basis of a shear stress intensity hypothesis (SIH) the material exposure is determined.

General stress conditions in the tooth

Inside the tooth, beneath an ideal smooth flank surface, the total stress conditions are composed of:

- stresses due to normal contact load (Hertzian theory);
- shear stresses on the surface caused by friction;

- thermal stresses caused by the thermal gradient;
- stresses caused by bending mechanism;
- residual stresses.

Figure 3 illustrates the stress components that influence the material exposure in a considered (infinite small) element. In Figure 3a the stress components that result from the normal load on the flank are shown. The stresses according to the Hertzian theory are arising out of the normal force. Due to the sliding components the friction force that is tangential to the flank surface induces shear stresses. Figure 3b demonstrates the effect of bending by a normal force that acts above the considered element (above in profile direction). The components of the normal force cause normal stresses with an approximately linear distribution over the tooth thickness and shear stresses with an approximately parabolic distribution and a maximum in the middle of the tooth. Residual stresses result from the hardening and finishing process. As an example, [20] shows compressive stresses are occurring in the case and are balanced by tensile stresses in the core. Unlike the stresses in Figure 3a and Figure 3b the residual stresses in Figure 3c are load independent.

Oster and Hertter developed the program system “STRORHR” for the calculation of all mentioned stress components on cylindrical gears. With this program it is possible to examine the material exposure in the subsurface below any contact point on the flank surface. Thereby the examination direction is perpendicular to the flank surface.

Stress conditions in the rolling contact

In any contact point on the flank the rolling direction x can also be seen as the time axis. Figure 4 shows in principle the stress components under the surface. All volume elements in the same depth are exposed to equal stresses, but at different times. To evaluate the material exposure in a certain depth beneath the flank surface the corresponding stresses have to be regarded over the whole time axis (x-axis).

However in rolling contacts a turning principal coordinate system complicates the evaluation of the material utilization. A possibility to analyze the dynamic stresses in rolling contacts are the shear stress courses in a sectional plane that is defined on the surface of the base sphere according to Figure 5.

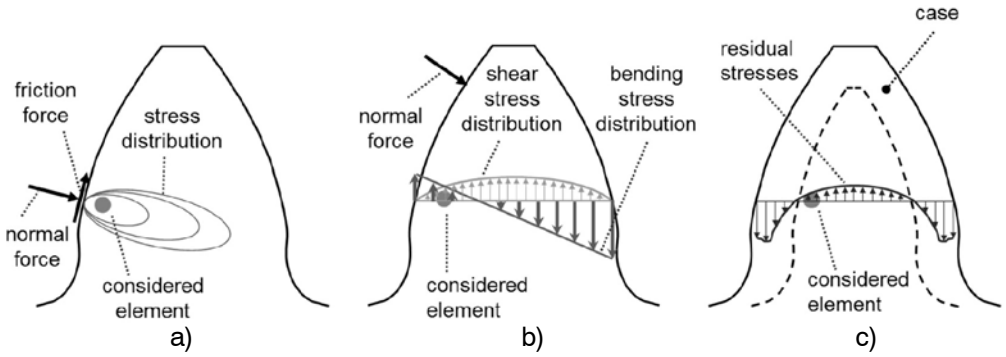

Figure 3. Stress conditions inside the tooth

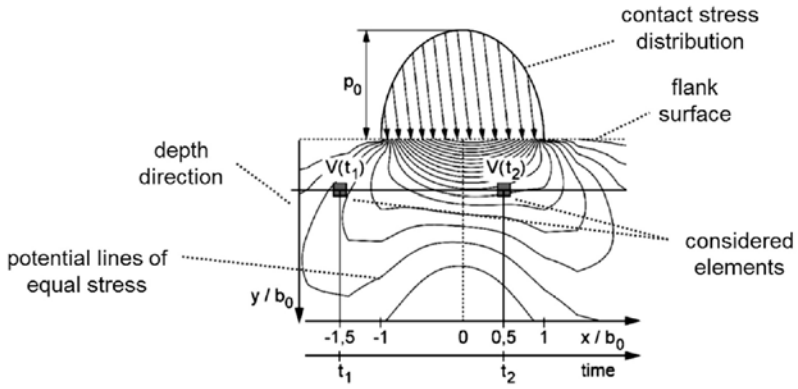

Figure 4. Time-dependent stress components in a rolling contact

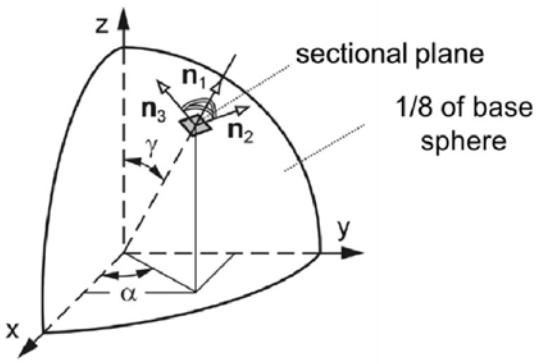

Figure 5. Base sphere with sectional plane [8]

Figure 6 shows for a rolling contact an example of shear stress courses in a certain sectional plane $\gamma\alpha$ and a material depth of $y/b_0 = 0.3$. $\tau\gamma\alpha(t_i)$ is the time dependent graph for the projection of shear stresses in the directions n_2 and n_3 (see Figure 5). In Figure 6a, no residual stresses are considered. As a consequence the point (0/0) is part of the course. At a certain time t_i, when the contact is still unloaded (e.g., the contact point of the flank surfaces is still far away from the regarded volume element) $\tau_2 = \tau_3 = 0$ in the examined sectional plane. During the movement of the contact over the flank surface the stress components τ_2 and τ_3 can be marked in the diagram. Of course if the influence of the moving contact point on the stresses at the examined plane is fading out the course will again reach the point (0/0). As Figure 6a shows, the instantaneous stress vector (τ_2/τ_3) is completely turning during one load cycle what means that it acts as an alternating load. Its maximum length is defined as the "maximum shear stress" $\tau_{max,a}$, the diameter of the circumscribed circle is $\Delta\tau_{max,a}$.

Figure 6b shows for the same examined sectional plane an equal load cycle but in consideration of the residual stresses. Unlike before the shear stresses τ_2 and τ_3 have discrete values even if the contact is unloaded. However the course of the pair of values τ_2/τ_3 is similar, what means that $\Delta\tau_{max,a} = \Delta\tau_{max,b}$. An important fact is, that the maximum shear stress $\tau_{max,b}$ is decreasing under the influence of (compressive) residual stresses ($\tau_{max,b} < \tau_{max,a}$). In other words the maximum shear stress with superposed compressive residual stresses is smaller than the maximum shear stress without residual stresses. This is also valid for other sectional planes of the base sphere and corresponds with the well-known fact, that compressive residual stresses reduce the maximum material exposure (e.g., [22]).

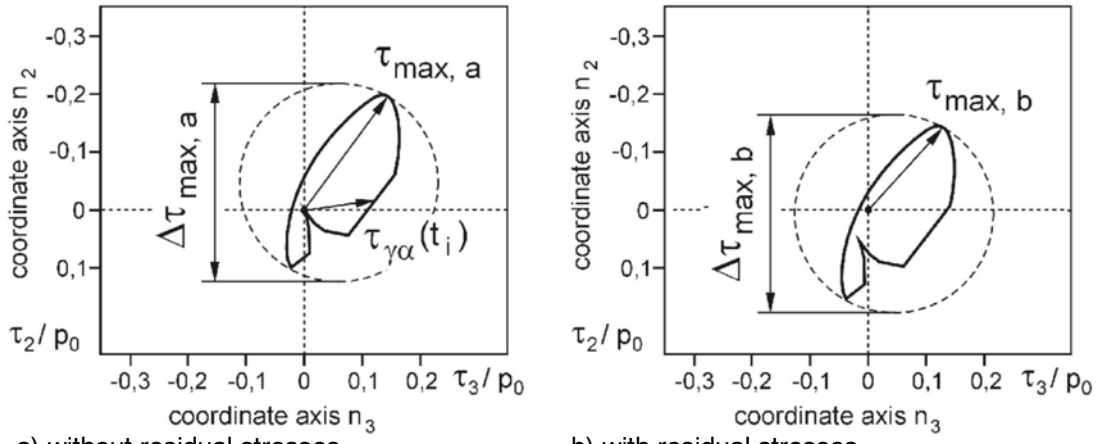

a) without residual stresses b) with residual stresses

Figure 6. Example of shear stress courses in a sectional plane $\alpha\gamma$ in the depth $y/b_0 = 0.3$ for rolling conditions [8]

The aim of strength hypotheses is the evaluation of the stresses occurring in the examined base sphere (or base element) to get a number for the material exposure that correlates well with the failure mechanism. Many common criteria are not applicable for alternating stresses as described before. Various important hypotheses are discussed to their applicability for the rating of the material exposure in rolling contacts. As a result of the investigation a modified shear stress hypothesis SIH was established [8]. The hypothesis can principally be used for:

- rating the maximum exposure of the material (analysis regarding yielding);
- rating the dynamic exposure of the material (analysis regarding fatigue).

New modified shear stress hypothesis by Hertter [8]

The base for the calculation of the decisive exposure in the examined base sphere are the stress courses in all sectional planes of the base sphere. According to [12], in every sectional plane the normal stresses (orthogonal to sectional plane) can be calculated according equations 3 and 4. The shear stresses $\tau\gamma\alpha_a$ and $\tau\gamma\alpha_m$ are defined as shown in Figure 7 for the considered sectional plane. The radius of the smallest circumcircle of the stress course is the decisive amplitude of the shear stress. The vector of its center point represents the mean shear stress.

Amplitude of shear stress, according to Figure 7

$$\tau\gamma\alpha_a = \tau_a(\gamma,\ \alpha) \tag{1}$$

Amplitude of shear stress, according to Figure 7

$$\tau\gamma\alpha_m = \tau_m(\gamma,\ \alpha) \tag{2}$$

Amplitude of normal stress, $\sigma\gamma\alpha_a = \sigma_a\ (\gamma,\ \alpha)$

$$\sigma_a(\gamma,\ \alpha) = \frac{\sigma_{max}(\gamma,\ \alpha) - \sigma_{min}(\gamma, \alpha)}{2} \tag{3}$$

Mean value of normal stress, $\sigma\gamma\alpha_m = \sigma_m\ (\gamma,\ \alpha)$

$$\sigma_m(\gamma,\ \alpha) = \frac{\sigma_{max}(\gamma,\ \alpha) + \sigma_{min}(\gamma, \alpha)}{2} \tag{4}$$

Dynamic exposure in sectional plane, $A\ (\gamma,\ \alpha)$

$$A(\gamma,\ \alpha) = \sqrt[\mu]{\frac{\alpha\ \tau_a^\mu \left(1 + m\ \tau_m^\mu\right) + b\ \sigma_a^\mu}{\sigma_A^\mu}} \tag{5}$$

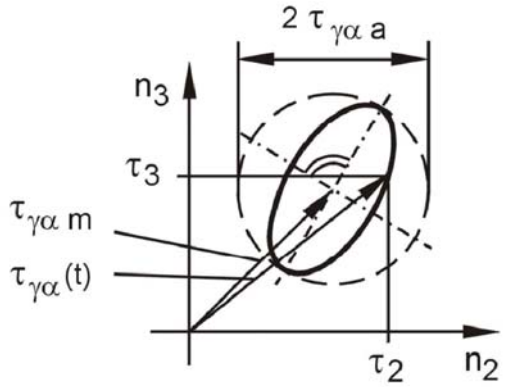

Figure 7. Definition of amplitude and mean value of any shear stress curve plotted over time in a discrete sectional plane [8]

Total dynamic exposure, $A_{\text{int a}}$

$$A_{\text{int a}} = \sqrt[\mu]{\frac{15}{8\pi} \int_{\gamma=0}^{\pi} \int_{\alpha=0}^{2\pi} \left(\left[A(\gamma, \alpha) \right]^2 \sin\alpha \right) d\alpha d\gamma} \tag{6}$$

Maximum exposure in sectional plane, $A_{\max}(\gamma, \alpha)$

$$A_{\max}(\gamma, \alpha) = \sqrt[\mu]{\frac{\alpha \tau_{\max}^{\mu} + b \sigma_{\max}^{\mu}}{R_{\text{p0,2}}^{\mu}}} \tag{7}$$

Total maximum exposure, $A_{\text{int a}}$

$$A_{\text{int a}} = \sqrt[\mu]{\frac{15}{8\pi} \int_{\gamma=0}^{\pi} \int_{\alpha=0}^{2\pi} \left(\left[A_{\max}(\gamma, \alpha) \right]^2 \sin\alpha \right) d\alpha d\gamma} \tag{8}$$

Constant a

$$a = \frac{1}{5} \left[3 \left(\frac{\sigma_W}{\tau_W} \right)^2 - 4 \right] \tag{9}$$

Constant b

$$b = \frac{1}{5} \left[6 - 2 \left(\frac{\sigma_W}{\tau_W} \right)^2 \right] \tag{10}$$

Constant m

$$m = \frac{1}{\alpha} \left[\frac{\sigma_W^2 - \left(\frac{\sigma_W}{\tau_W} \right)^2 \left(\frac{\tau_{\text{Sch}}}{2} \right)^2}{\frac{12}{7} \left(\frac{\tau_{\text{Sch}}}{2} \right)^4} \right] \tag{11}$$

where

$\tau_a(\gamma,\alpha)$	is amplitude of shear stress in sectional plane, N/mm^2;
γ	is angle for sectional plane (Figure 5), degrees;
α	is angle for sectional plane (Figure 5), degrees;
$\tau_m(\gamma,\alpha)$	is mean value of shear stress in sectional plane, N/mm^2;
$\sigma_a(\gamma,\alpha)$	is amplitude of normal stress in sectional plane, N/mm^2;
$\sigma_{max}(\gamma,\alpha)$	is maximum of normal stress in sectional plane, N/mm^2;
$\sigma_{min}(\gamma,\alpha)$	is minimum of normal stress in sectional plane
$\sigma_m(\gamma,\alpha)$	is mean value of normal stress in sectional plane, N/mm^2;
$A(\gamma,\alpha)$	is dynamic exposure in sectional plane;
μ	is constant exponent $\mu = 2$;
b	is constant (material–dependent);
σ_A	is material amplitude strength according to normal stress, N/mm^2 [8];
$A_{\text{int a}}$	is total dynamic exposure of base sphere;

$A_{max}(\gamma,\alpha)$ is maximum exposure in sectional plane;

$R_{p0,2}$ is yield strength, N/mm^2

A_{int} is total maximum exposure of base sphere;

a is constant (material-dependent);

σ_W is material alternate strength according to normal stress, N/mm^2 [8];

τ_W is material alternate strength according to shear stress, N/mm^2 [8];

m is constant (material-dependent);

τ_{Sch} is material pulsating fatigue strength, N/mm^2 [8];

With the stress values according to equations 1 through 4 the material exposure $A(\gamma,\alpha)$ in the considered sectional plane can be calculated [8]. The local amplitude strength σ_A is dependent of the mean value of normal stress $\sigma_m(\gamma,\alpha)$. The constants a, b and m are a function of the strength ratio σ_W/τ_W and the local torsional pulsating fatigue strength τ_{Sch} [12].

The total dynamic exposure $A_{int\,a}$ is defined as the integral value of the exposure values $A(\gamma,\alpha)$ in all sectional planes and determined by equation 6. The endurance limit of the considered element regarding fatigue is per definition reached when the total dynamic exposure becomes $A_{int\,a} = 1$. Values below stand for infinite life. In an analogous way the maximum exposure regarding yielding is calculated (equation 7). For all sectional planes in the base sphere the total maximum exposure for yielding is considered according to equation 8. Again for an infinite life the total maximum exposure has to fall below $A_{int} < 1$.

It is remarkable that all local strength values can be determined out of the Vickers hardness values by means of material-physically based relations. For details see [8].

Calculation process for bevel and hypoid gears

Overview

As described above, Hertter [8] developed for cylindrical gears the material-physically based method to evaluate the material exposure in the subsurface of the tooth. The strength values are thereby derived from the Vickers hardness in the regarded volume element (base sphere).

The comparison of the local stress values with the local strength values provides a 3-dimensional evaluation of the material exposure: Not only close to the flank surface but also in an area close to the core. Whereas the allowable stress numbers according to ISO, DIN or AGMA are only valid for an optimally designed case depth, the material-physically based method allows the investigation of the influence of different hardness profiles on the load capacity. Moreover due to the local consideration of the material exposure the failure mode becomes apparent.

Hertter expanded the computer program ROSLCOR (Rolling and SLinding Contact according to OsteR. [9] [17]) that was developed at the FZG (Gear Research Center of the Technical University of Munich) with his material-physically based method. Wirth [20] transferred the Hertter's method to bevel and hypoid gears. Wirth developed the computer tool LokAna (Local Analysis) that handles not only the subprograms BECAL [10] and ROSLCOR but does also further calculations for bevel gears.

Calculation of the material exposure

The Hertzian stresses on the flank surface of bevel and hypoid gears are determined with the FVA-program BECAL (Bevel Gear Calculation) [10]. With the machine settings for the gear set BECAL is able to generate the geometry of the flank surface and the tooth root. Based on this a loaded tooth contact analysis leads to the tooth root stresses and to the local occurring Hertzian stresses. Deflections of housing, bearings and shafts can be also considered.

For any calculated point on the flank the partial line of contact, its relative curvature, the acting normal force and the Hertzian stress is determined. For ROSLCOR, the considered contact point can be simplified to a contact of an infinite long cylinder with a half-plane, as it can be seen in Figure 8.

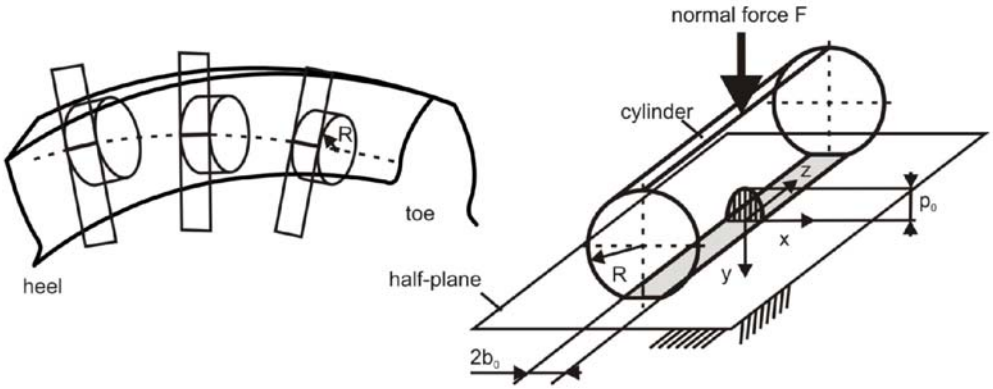

Figure 8. Simplification of the complex contact conditions to a cylinder model

In the stress calculation with ROSLCORHR [8] which is an advancement of ROSLCOR, the normal stresses and shear stresses resulting from bending (Figure 3b) are regarded. The acting normal force that moves over the flank surface causes at any later stage normal stresses and shear stresses in the considered volume element (base sphere). For the material exposure the maximum values over one load cycle have to be considered.

The stresses caused by the normal load in the subsurface are calculated with the model shown in Figure 8 on the right. Basis for the stress mechanics is the plain strain state. This means that deformations are only allowed in a plane vertical to the contact line. ROSLCOR considers the normal pressure on the surface as well as the influence of a loss of friction contact. The influences of thermal stresses and shear stresses on the material exposure are also regarded.

The material–physically based calculation model evaluates for a certain volume element the risk for an initial crack. Whether the crack will result in a damage of the flank or not is dependent on the potential for crack growth. Especially nearby the flank surface this potential is affected by the slip conditions in the contact point. As well–known [14] [19] pitting occur mainly in the flank area with negative slip, which is below the pitch point for pinion and wheel at bevel gears without offset. Deeper below the flank surface the influence of slip in the contact point seems, as known so far, negligible.

Wirth [20] introduced a so called slip factor that accounts for the difference in strength between negative and positive slip conditions. The influence of this factor is restricted to the material close to the surface. Because the material strength values are derived from the material hardness, it is practicable to increase (virtually) the hardness values appropriately. Consequently for the same load conditions the material exposure in flank areas with positive slip is lower than in areas with negative slip. The hardness values are modified by equations 12 through 14. Wirth demonstrated that reasonable results are calculated if $a/b_0 = 0.5$ and $b/b_0 = 1.0$ is chosen (b_0: half of the Hertzian contact width according to Figure 8).

Depth range $0 < y < a$:

$$HV(y) = HV_0(y)\, Z_{S1,2} \tag{12}$$

Depth range $y > b$:

$$HV(y) = HV_0(y) \tag{13}$$

Depth range $a \leq y \leq b$.

Linear interpolation of Z_S (14)

where

y is material depth below the contact point, mm;

a is certain material depth, mm;

$HV(y)$ is modified local hardness in consideration of the slip influence, HV;

$HV_0(y)$ is local hardness, HV;

b is certain material depth, mm;

Z_S is factor according to [20].

Residual stresses in the tooth

Hertter demonstrated that the influence of residual stresses has to be considered in the material exposure (see Figure 6) for the evaluation of tooth failures. Particularly the maximum material exposure A_{int} is influenced by the residual stresses. Whereas compressive stresses have usually a positive effect on the material exposure, tensile stresses increase the material stresses [8]. The total dynamic exposure $A_{int\,a}$ is only influenced by means of the mean stress sensitivity. As Hertter proved the material exposure in the range of the transition zone from case to core accounts for failure modes like flank breakage that are usually characterized by an initial crack in this region.

Wirth [20] proposes to adopt the (compressive) residual stresses according to Lang [11] for the case. Due to the balance of forces in the core tensile residual stresses have to exist. For the estimation of the residual stress distribution in the core Wirth made investigations on basis of FE-methods. Using a parabola of 4th degree, the tensile stresses can be approximated well by the balance of forces. Figure 9 shows qualitatively in a normal section of the tooth the residual stress distribution. It is a sufficient correlation that the residual stresses in tooth height direction are equal to the residual stresses in lengthwise direction. Residual stresses that are directed orthogonal to the flank surface are neglected.

Improvement of a gear set with flank breakage

Wheel flank breakage

A decisive number of hypoid gear sets used in axle gear drives in test vehicles failed of flank breakage. Only the wheels were affected by this failure mode. Figure 1 (left side) shows a flank breakage on one tooth of a wheel, in Figure 1 (right side) pitting on the coast side could be detected. Figure 2 shows on another wheel a characteristic flank breakage. As it can be seen the failure plane runs on both flank sides through the active tooth height.

To learn more about the conditions where and when flank breakages occur a new type of test for the stationary test rig has been developed. Comprehensive test runs have been made. The gears sets have been tested for a defined load spectrum where the highest load stage was the torque that has been considered in the following calculations. The gear sets failed either by pitting or flank breakage. Pitting occurred on the pinion as well as on the wheel. Flank breakage was only observed on the wheel.

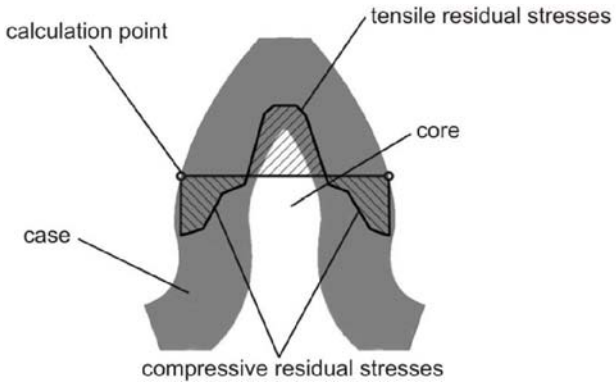

Figure 9. Residual stress distribution in the tooth

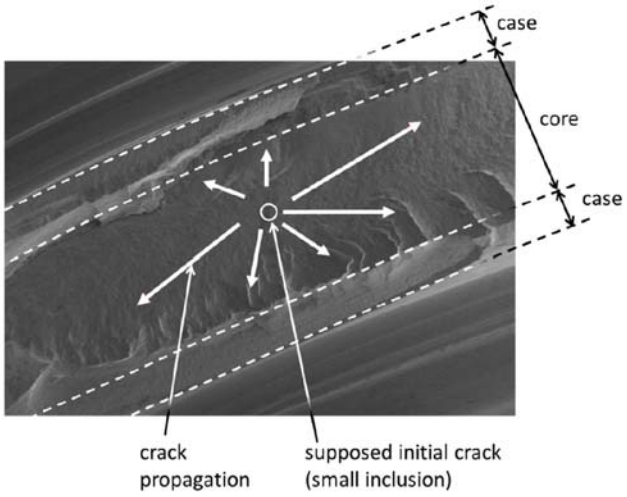

Figure 10. Flank breakage on two different wheels

Figure 10 shows for a damaged wheel the investigation of the fracture surface in the scanning electron micrograph. In this case a small inclusion was detected where–from the crack propagates to the flank surfaces. Inclusions can be regarded as a catalyst for the crack initiation because of the notching effect of different elasticity modulus. Investigations of Annast [1] showed that an Al_2O_3–inclusion causes a stress increase (von–Mises criterion) of approximately 30%–40%. The size and the depth beyond the surface have a relatively small influence. Therefore, the lower the material exposure in the core can be realized, the smaller the risk of flank breakage with initial cracks in this region will be, as Figure 10 demonstrates.

Design of an improved gear set

The aim of the redesign was to develop a new gear design with a smaller material exposure to avoid flank breakage on the one hand and pitting as far as possible on the other hand. In a first step the old design was analyzed with the new introduced material–physically calculation method. In the second step a new gear design with same ratio and diameters but lower material exposure was searched by an iterative process. Table 1 contains the main geometry data of the old and the new gear design.

NOTE: Because only the wheel was affected by flank breakage all calculations have been made for the wheel only!

Table 1. Geometry of the examined gear sets

Nomenclature	Symbol	Unit	Old design		New design	
			Pinion	Wheel	Pinion	Wheel
Number of teeth	z	– –	8	45	8	45
Pinion offset	a	mm	34		34	
Normal module	m_{mn}	mm	6.134		6.122	
Mean pitch diameter	d_m	mm	69.6	331.2	69.9	332.3
Face width	b	mm	60.7	58.3	62.2	59.0
Spiral angle	β	°	45.5	34	45.5	34
Material	– –	– –	25MoCr4E		25MoCr4E	
Roughness Rz flank/tooth root	Rz	mm	3/16 (after run in)			
Total overlap ratio (under load) drive/coast	– –	– –	3.0/2.7		2.92/2.7	
Lubricant	– –	– –	Shell Spirax ASX 75W 90			
Temperature of lubricant	ϑ	°C	90			

For the calculation discrete contact points on the flank have to be chosen for the evaluation. As Figure 11 shows the selected contact points are positioned in a section with considerably high load and the supposed crack origin. To evaluate not only the risk of an initial crack at one single point but also the potential of crack growth four different positions were examined.

Table 2 contains the Hertzian stresses that were determined by means of the loaded tooth contact analysis with BECAL [10]. Deformation and deflections of housing, shafts and bearings have been considered. Under the same load conditions it was possible to reduce the stresses on both flank sides in the critical area of the flank by approximately 15%. This was possible with an optimized crowning (Ease-Off) in combination with a different gear design (duplex instead of semi completing) and changed pressure angles.

Of course the reduction of contact stresses leads in most cases to an increase in load capacity, especially when the failure mode pitting is regarded. But in case of flank breakage the failure mechanism is not influenced only by the contact stresses but also by the material exposure deep inside the tooth. Because of the requirement to keep the amount of transferred torque by remaining the gear dimensions (and module) the flank load in total cannot be significantly reduced. To avoid flank breakage it has to be the aim to reduce material exposure mainly in the core where in this case the crack initiation could be detected in several cases (see Figure 10).

As mentioned earlier in the evaluation of the material exposure in the subsurface section, especially in the middle of the tooth thickness, the following stress components may not be disregarded:

- shear stresses due to the shearing forces (flank normal forces);
- tensile residual stresses.

The shear stress distribution reaches its maximum in the middle of the tooth thickness as shown in Figure 3b. Also the maximum values of the tensile residual stresses are supposed to be in this region. Whereas the determination of the shear stresses is only a mechanical problem, the residual stresses are caused mainly by the heat treatment process. Only in the area direct beneath the surface residual stresses are influenced by the finishing process of the gear. Due to this the residual stresses are derived by the hardness profile as described earlier.

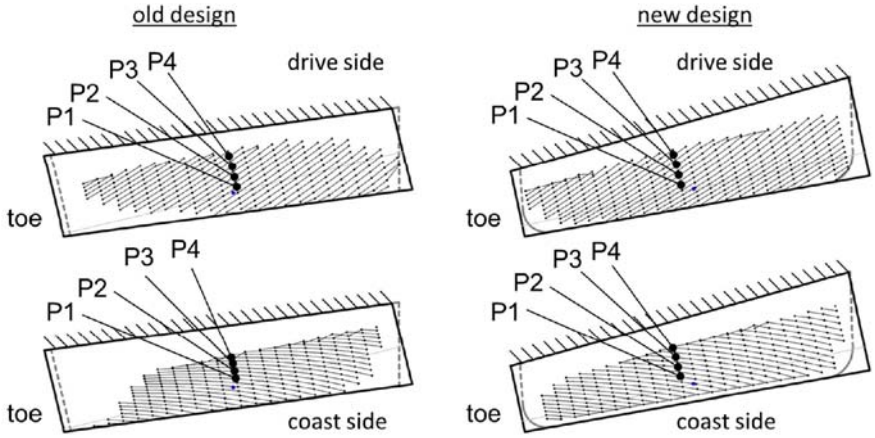

Figure 11. Contact pattern and calculated contact points on the wheel flanks

Table 2. Hertzian stress under the considered load

Calculation point	Old design		New design	
	Drive side	Coast side	Drive side	Coast side
P1	1865	1951	1629 (-13%)	1692 (-13%)
P2	1891	1979	1571 (-17%)	1698 (-14%)
P3	1841	1961	1593 (-13%)	1651 (-16%)
P4	1612	1901	1553 (-4%)	1585 (-17%)

Figure 12 shows for the calculations results presented in the following the assumed hardness profiles, that are based on detailed measurements but smoothed for calculation. Because of the slightly different cooling conditions during the hardening process in profile direction of the tooth the hardness gradients and the core hardness are slightly different. The derived residual stress distributions are shown as well in Figure 12. As it can be seen the compressive stresses in the case are up to $\sigma_{res} \approx 400$ N/mm^2 and are decreasing until the transient region of case and core. Because the case thickness in profile direction is more or less constant the compressive residual stress profiles are similar. In contrast to that the tensile residual stresses in the middle of the tooth thickness are increasing from point P4 to P1. The reason is the mechanical balance of forces: The separating forces that are caused by the compressive stresses in the case are approximately constant for P1 to P4. The attracting force is represented by the tensile compressive stresses and has to have an equal amount. Because the core section becomes smaller from P4 to P1 the corresponding tensile stresses have to increase.

In Figure 13, the calculated material exposure for point P1 to P4 are shown. The black lines represent the total dynamic exposure $A_{\text{int a}}$ and the grey lines the total maximum exposure A_{int}.

$A_{\text{int a}}$ can be seen as a value to describe the material fatigue. It is based on an endurance strength (derived from the Vickers hardness) for a failure probability of 50%. Pitting is a typical fatigue failure that correlates with the total dynamic exposure $A_{\text{int a}}$. [8], [18] and [20] show that if material exposure values exceed a certain limit in the subsurface up to a depth of $y/b_0 \approx 1$ (b_0: half of Hertzian contact width) pitting failure occur with a high probability. For the examined gear this decisive range is up to approximately $y \approx 1$ mm. As Figure 13 shows $A_{\text{int a}}$ exceeds the limit of "1". Due to the load spectrum of the test vehicles which had only a few time slices with this considered load pitting failures on the drive side where not detected. The fatigue strength may be the reason for that.

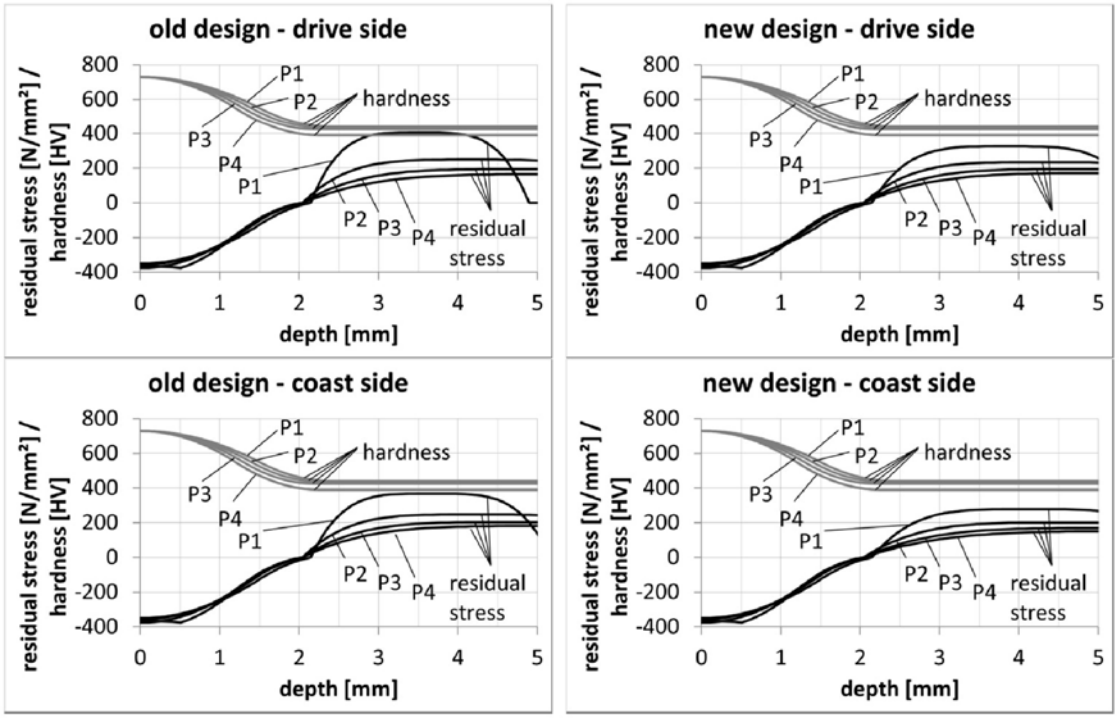

Figure 12. Profiles for hardness and residual stress

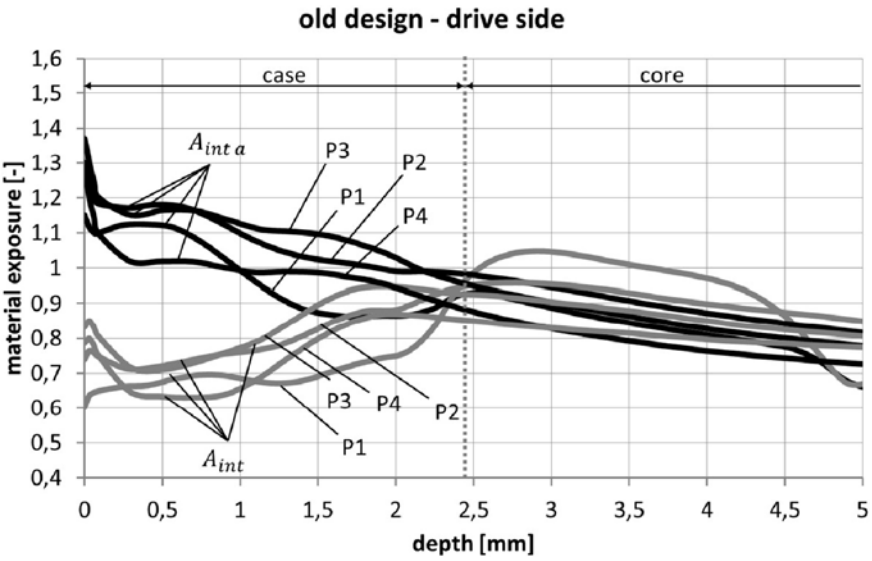

Figure 13. Material exposure for calculated points: <u>old</u> design – drive side of wheel

A_{int} represents the material exposure concerning yielding. According to the theory of the calculation method if $A_{int} > 1$ local redistribution of stress or initial cracks occur. This situation is tightened if the notching effect of inclusions or discontinuities increases the material exposure. At this time there is no possibility provided by the material-physically based method to regard this fact in the calculation process. Therefore the practical limit for A_{int}-values that are determined for a homogenous material should be reduced to values smaller than "1" in order to be on the safe side. Because of the specifics of the hardening process discontinuities occur more typically in the core than in the case. This is why the total maximum exposure A_{int} should be limited especially in the core.

Hertter [8] and Wirth [20] found a good correlation between the total maximum material exposure A_{int} and the failure mode flank breakage: Especially high values in the material depth between the transition of case and core as well as in the core seem to be responsible for flank breakage. It has to be mentioned that crack initiations that are caused by yielding have no endurance limit or fatigue strength for finite life. According to theory only very few single load cycles are enough for stress redistribution or crack initiation. These cracks may have the ability to grow also at lower loads! Unlike for the calculation against fatigue where there is a high strength for finite life, it is already critical if an initial crack occurs during a momentary high load. In other words, it is more important to reduce high A_{int}-values (concerning yielding) than the $A_{int\,a}$-values (concerning fatigue) if the gear set is stressed by an load spectrum with only momentary high loads.

As Figure 13 shows A_{int} of P1 exceeds the limit "1" in the depth between y = 2.5...3.7 mm. Point P2 causes values $A_{int} > 0.9$ in a range between y = 2.2...4 mm and P3 for y = 1.5...3.2 mm. Only the A_{int}-graph for P4 is constantly under 0.9. These high values of A_{int} over a considerable big section of the tooth correlate well with the witnessed flank breakages.

For the appearance of flank breakage it is not necessarily sufficient that yielding starts in one single volume element. Local peaks of material exposure may be reduced after a yielding process and no growing crack is initiated. This means that the failure mode of flank breakage will not occur. Therefore it is not only decisive for flank breakage if in one contact point the limit for yielding is reached. In fact high values of A_{int} in adjacent contact points support the growth of cracks. To evaluate this potential a mean value of the total maximum exposure is defined according to equation 15. For the four considered contact points the average value of each A_{int}-graph is determined in a certain depth. Of course on basis of this consideration the determination of the $A_{int\,a}$-mean value is also reasonable to get an imagination of the pitting danger over the considered flank area.

$$\overline{A}(y) = \frac{1}{i}\sum_{1}^{i} A_i(y) \tag{15}$$

where

$\overline{A}$ is mean value of total dynamic exposure $A_{\text{int a}}$ or mean value of the total maximum exposure A_{int};

y is material depth, mm;

i amount of considered calculation points;

A is total dynamic exposure $A_{\text{int a}}$ or total maximum exposure A_{int}.

In Figure 14 the graphs of the mean values $\overline{A_{\text{int a}}}$ and $\overline{A_{\text{int}}}$ are shown for the drive side of the wheel flank. It is obvious that in the depth y < 1 mm $\overline{A_{\text{int a}}}$ has considerable high values. As mentioned before this is an explanation for the observed pitting in the field. But more important for flank breakage is, as described before, the profile of $\overline{A_{\text{int}}}$. It can be seen in Figure 14 that in the depth y = 2.3...3.7 mm the exposure is $\overline{A_{\text{int}}} \geq 0.9$ Together with the mentioned influence of inclusions like detected according to Figure 10 it is obvious that there is a high risk of flank breakage under this load conditions. The profiles for hardness and residual stress shown in Figure 14 are also principally derived by equation 15 and hence can be understood as the mean values.

Figure 15 shows for the new design the corresponding calculations for point P1 to P4. Compared to Figure 13 it is obvious that in the close region to the surface (y < 1 mm) the total dynamic exposure $A_{\text{int a}}$ could be reduced. But more important for the failure mode flank breakage is the reduction of the total maximum exposure A_{int} in the subsurface of the tooth: The exposure profiles of all considered points do not exceed the theoretical limit of “1”. Furthermore the maxima of A_{int} for the points P1 to P2 are significantly lower.

In Figure 16 the mean values according equation 15 are shown for the drive side of the new design. As mentioned before their values represent the potential for growing cracks. It can be seen that in the relevant depth for pitting (y < 1.0 mm) there is a significant reduction of the total dynamic exposure $\overline{A_{\text{int a}}}$. For better illustration the profile of the old design is shown by the dotted line. The improvement for pitting can be estimated with approximately 15%. Again the mean values show also the reduced crack growth potential in the inner of the tooth. In the transition from case to core the values for the total maximum exposure $\overline{A_{\text{int}}}$ are lowered by approximately 14%.

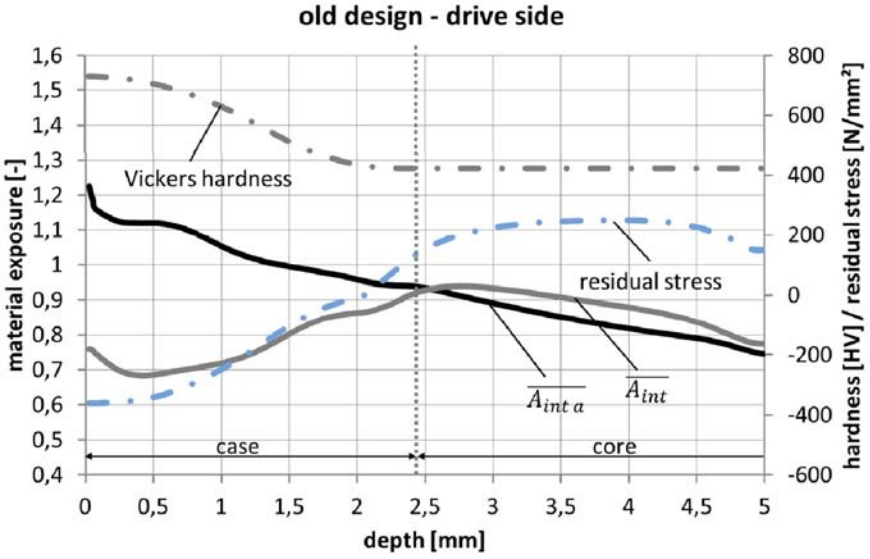

Figure 14. Mean values of material exposure (crack growth potential): old design – drive side of wheel

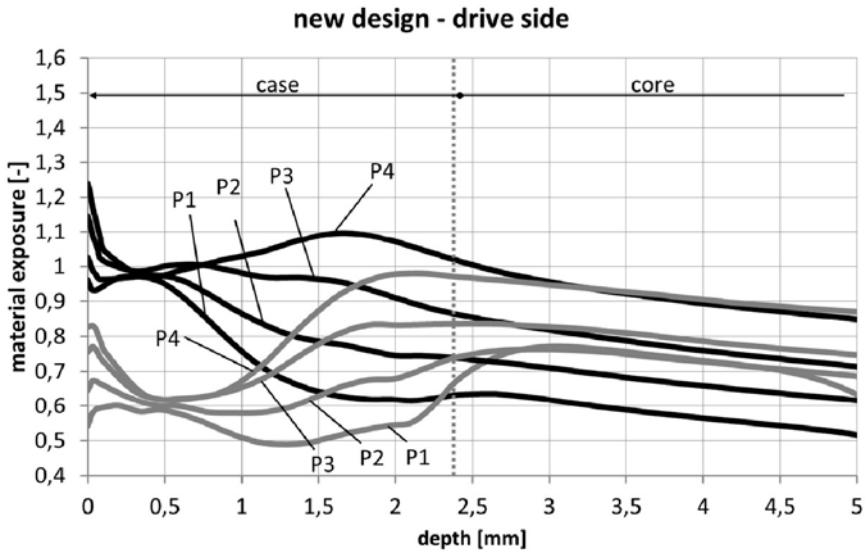

Figure 15. Material exposure for calculated contact points: <u>new</u> design – drive side of wheel

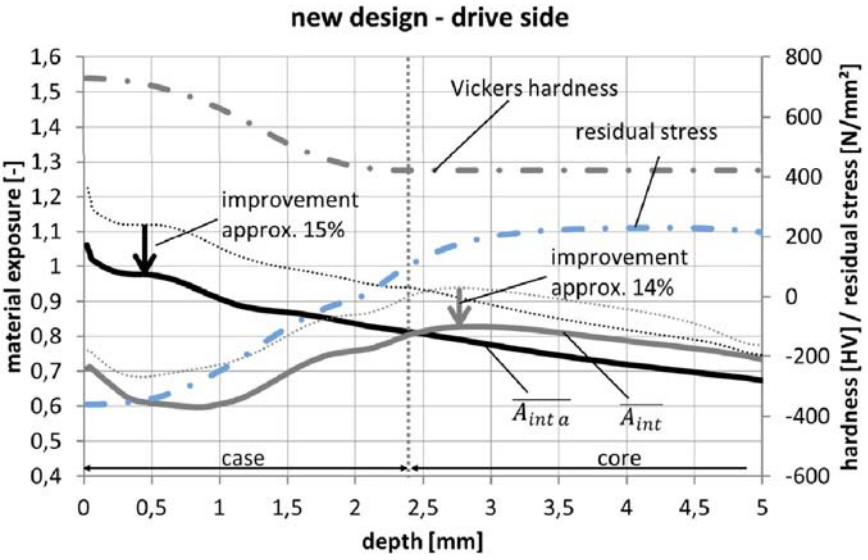

Figure 16. Mean values of material exposure (crack growth potential): new design – drive side of wheel

Finally it can be stated for the drive side flanks of the new design that the exposure profiles $A_{\text{int a}}$ and A_{int} that represent the risk of crack initiation are significantly lower as well as the mean values $\overline{A_{\text{int a}}}$ and $\overline{A_{\text{int}}}$ that can be regarded as the potential of crack growth.

Of course it is not sufficient to optimize only the drive side flanks. The specific load spectra in the practical field show that the coast side flanks are considerably high loaded. Hence the coast side is analyzed with the same load as the drive side.

Figure 17 and Figure 18 show the comparison of the exposure profiles for the old and new gear design for the coast side flanks. As on the drive side the values of $A_{\text{int a}}$ in the decisive depth for pitting could be significantly reduced. But also in the decisive depth for flank breakage where the initial crack is supposed (see Figure 10) the maximum exposure A_{int} could be lowered in every considered calculation point.

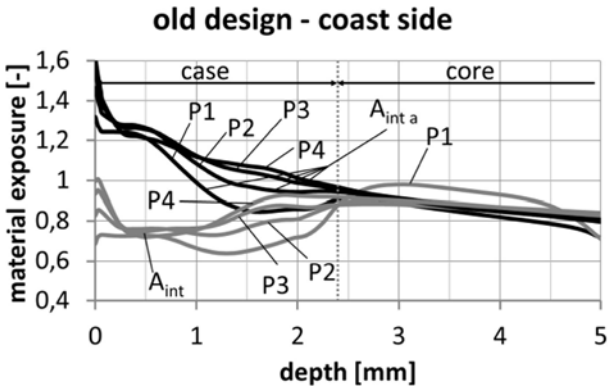

Figure 17. Material exposure for calculated contact points: old design – coast side of wheel

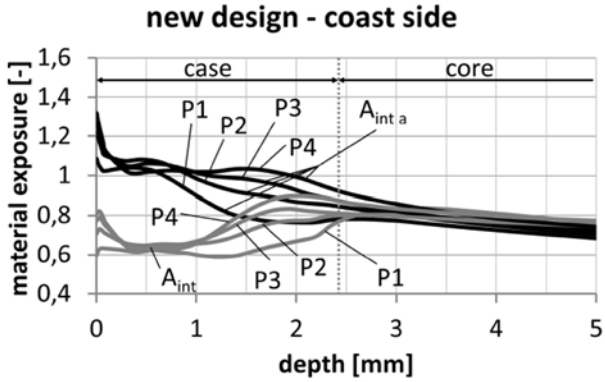

Figure 18. Material exposure for calculated contact points: new design – coast side of wheel

For the old design the mean values of the exposure profiles are shown in Figure 19. As it can be seen the $\overline{A_{\text{int a}}}$ level regarding pitting (y < 1.0 mm) is even higher than for the drive side. This correlates well with pitting that were observed on several gears of the test vehicles (see Figure 1). Regarding the crack growth potential for flank breakage the mean values for the exposure $\overline{A_{\text{int}}}$ are similar to those on the drive side. This means that initial cracks close to the middle of the tooth thickness can grow for drive side loading as well as for coast side loading.

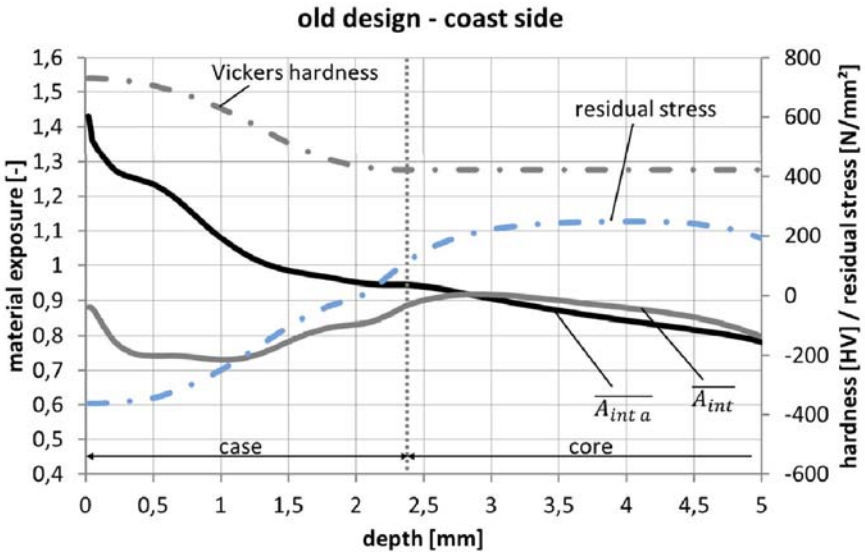

Figure 19. Mean values of material exposure (crack growth potential): old design – coast side of wheel

As Figure 18 proves the decisive $A_{int\,a}$-values for pitting could be clearly decreased, what is confirmed also by the mean values $\overline{A_{int\,a}}$ shown in Figure 20. Furthermore the risk of crack initiation in the subsurface y > 1.5 mm is lowered for every considered point (see Figure 18). Of course this leads to an improved situation for the crack growth potential. As shown in Figure 20 the mean values $\overline{A_{int}}$ could be reduced by approximately 11% with the new design.

Because of the positive prediction in load capacity, especially concerning flank breakage and pitting, prototype gear sets based on the new design have been produced and were analyzed in the test rig. The gears were loaded by the same load spectrum. The main aim to avoid flank breakages under these conditions was reached in any case. Moreover pitting on wheel flanks did not occur during the tests. Though the pinion is now failing by pitting, the run time could be stretched by approximately the factor 4.

Summary

Flank breakage occurred on the wheel of several bevel gears sets used in test vehicles of MTB. In some cases the damage was accompanied by pitting on several wheel flanks. A couple of tests on a MTB test rig showed that this type of failure is reproducible for a certain load spectrum.

It was the aim of a new gear design to avoid flank breakages in any case and to increase the load capacity regarding pitting. Because it was essential to keep the outer wheel diameter, the pinion offset and the gear ratio mostly the micro geometry of corresponding flanks (Ease-Off) was modified. To reduce the amount of test gears during the redesign process a new calculation model was used to evaluate the risk for flank breakage and pitting on basis of a loaded tooth contact analysis.

The new calculation model was introduced by Hertter [8] for cylindrical gears and expanded by Wirth [20] taking in consideration the specifics of bevel and hypoid gears. The method is based on material-physical relationships and allows the evaluation of the material exposure in the subsurface. The influences of local hardness (via hardness profile) and residual stresses can be considered. As demonstrated in [18], [8] and [20], the material exposure in the depth close to the surface is decisive for pitting failure. In contrast to that high material exposure in the transient region from case to core or in the middle of the tooth thickness seems to affect flank breakage.

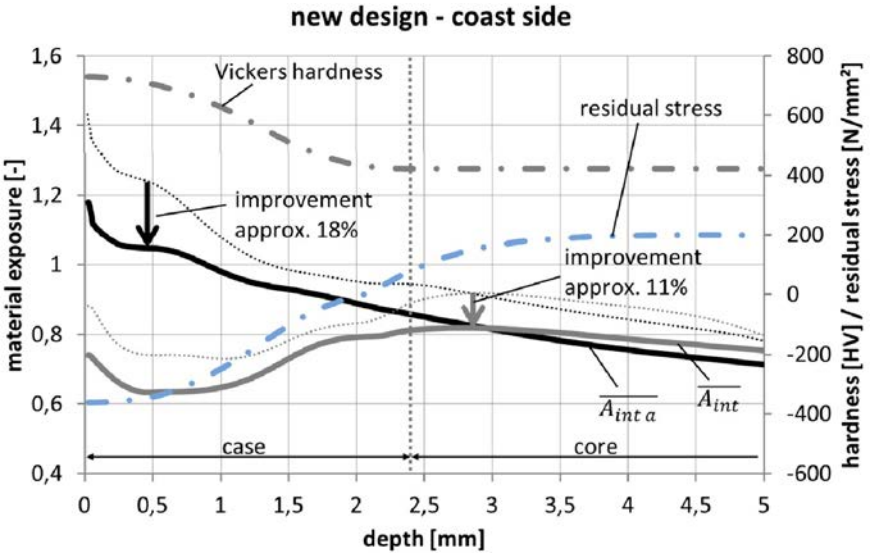

Figure 20. Mean values of material exposure (crack growth potential): <u>new</u> design – coast side of wheel

With the new model the risk of pitting and flank breakage failures can be evaluated. Whereas the pitting resistance can be predicted sharply, an assured calculation of the load capacity regarding flank breakage is hardly possible. Uncertainties in the calculation model are the influences of inclusions or material discontinuities on the material exposure. Furthermore the tensile residual stresses that have a decisive influence are only estimated by a simple model. FE–analysis could improve the prediction quality of the model. Nevertheless the comparison of load capacity of two gear designs produced in a similar way is reliably possible.

In an iterative process new gear designs have been analyzed with the material–physical calculation method. The result is a new gear set with a significant lower risk of failing by pitting or flank breakage. Test with first prototype gear sets confirmed the improvement. Neither pitting nor flank breakage occurred during the previous test runs.

References

[1] Annast, R., Kegelrad–Flankenbruch. Diss. TU München.

[2] ANSI/AGMA 2003–B97, *Rating the Pitting Resistance and Bending Strength of Generated Straight Bevel, Zerol Bevel, and Spiral Bevel Gear Teeth*

[3] Batista, A.C., Dias, A.M., Lebrun, J.L., Le Flour, J.C., Inglebert, G., *Contact fatigue of automotive gears, evolution and effects of residual stresses introduced by surface treatments*. Fatigue Fract. Engng. Mater. Struct. 23 (2000), S. 217 – 228.

[4] Coleman, W., *Bevel and Hypoid Gear Surface Durability, Pitting and Scuffing*. Institution of Mechanical Engineers, Paper 13 of Proceedings 1967–69, Volume 182, Part 3A, Gleason Works, Rochester, NY.

[5] Dudley, D.W., Winter, H., *Zahnräder - Berechnung, Entwurf und Herstellung nach amerikanischen Erfahrungen*. Springer Verlag, Berlin, 1961.

[6] Elkholy, A., *Case Depth Requirements in Carburized Gears*. Wear 88 (1983), S. 233–244.

[7] Gärtner, J., *Betriebsverhalten hochbelasteter Kegelradsätze in Traktoren. Berichtsband zur Tagung Innovationen rund ums Kegelrad,* Aachen, 10.–11.3.1998.

[8] Hertter, T., *Rechnerischer Festigkeitsnachweis der Ermüdungstragfähigkeit vergüteter und einsatzgehärteter Stirnräder*. Diss. TU München, 2003.

[9] Höhn, B.–R., Oster, P., *Der Flankenkontakt - ein elastohydrodynamischer Wälzkontakt.* VDI–Berichte 1207 (1995), S. 93 – 106.

[10] Hutschenreiter, B., *Ergänzung der Berechnungsmöglichkeit von BECAL für Flanken mit negativem Höhenballigkeitsradius und Kopfrücknahme*. Abschlussbericht und Handbuchergänzung D zur Version 3.4.0. FVA–Forschungsheft Nr. 548, Forschungsvereinigung Antriebstechnik e.V., 2007.

[11] Lang, O.R., *Berechnung und Auslegung induktiv randschichtgehärteter Bauteile*. In, Kloos, K.H. (Hrsg.), Grosch, J. (Hrsg.), Induktives Randschichthärten, Tagung 23. bis 25. März 1988, München, AWT, 1989, S. 332 – 348.

[12] Liu, J., *Beitrag zur Verbesserung der Dauerfestigkeitsberechnung bei mehrachsiger Beanspruchung.* Dissertation TU Clausthal, 1991.

[13] Pederson, R., Rice, R.L., *Case Crushing of Carburized and Hardened Gears*, Trans. SAE, 1961, S. 360–370.

[14] Rösch, H., *Untersuchungen zur Wälzfestigkeit von Rollen – Einfluss von Werkstoff, Wärmebehandlung und Schlupf*. Diss. TU München, 1976.

[15] Sandberg, E., *A Calculation Method for Subsurface Fatigue.* International Symposium on Gearing and Power Transmissions, Tokyo 1981, Volume 1, S. 429–434.

[16] Sharma, V.K., Breen, D.H., Walter, G.H., *An Analytical Approach for Establishing Case Depth Requirements in Carburized and Hardened Gears*, Transaction of ASME for presentation at the Design Engineering Technical Conference, Chicago, Illinois, September 26–30, 1977.

[17] Oster, P., *Beanspruchungen der Zahnflanken unter Bedingungen der Elastohydrodynamik.* Dissertation TU München, 1982.

[18] Tobie, T., *Zur Grübchen- und Zahnfußtragfähigkeit einsatzgehärteter Zahnräder*. Dissertation TU München, 2001.

[19] Wirth, C., *Entwicklung eines Berechnungsverfahrens zur Grübchen- und Zahnfußtragfähigkeit von Hypoidrädern*. Forschungsvereinigung Antriebstechnik e.V., Heft 887, Frankfurt 2009.

[20] Wirth, C., *Zur Tragfähigkeit von Kegelrad- und Hypoidgetrieben*. Diss. TU München, 2008.

[21] Zenner, H., Richter, I., *Eine Festigkeitshypothese für die Dauerfestigkeit bei beliebigen Beanspruchungskombinationen*. Konstruktion 29 (1977), S. 11 –18.

[22] Zwirlein, O., Schlicht, H., *Werkstoffanstrengung bei Wälzbeanspruchung – Einfluss von Reibung und Eigenspannungen*. Z. Werkstofftech. 11 (1980), S. 1 – 14.